Journal of Visualized Experiments

Spot Variation Fluorescence Correlation Spectroscopy for Analysis of Molecular Diffusion at the Plasma Membrane of Living Cells

--Manuscript Draft--

Article Type:	Invited Methods Article - JoVE Produced Video
Manuscript Number:	JoVE61823R1
Full Title:	Spot Variation Fluorescence Correlation Spectroscopy for Analysis of Molecular Diffusion at the Plasma Membrane of Living Cells
Corresponding Author:	Tomasz Trombik Uniwersytet Wroclawski Wydzial Biotechnologii Wroclaw, dolnoslaskie POLAND
Corresponding Author's Institution:	Uniwersytet Wroclawski Wydzial Biotechnologii
Corresponding Author E-Mail:	tomasz.trombik@uwr.edu.pl
Order of Authors:	Sebastien Mailfert
	Karolina Wójtowicz
	Sophie Brustlein
	Ewa Blaszczak
	Dr Nicolas Bertaux
	Marcin Łukaszewicz
	Didier Marguet
	Tomasz Trombik
Additional Information:	
Question	**Response**
Please indicate whether this article will be Standard Access or Open Access.	Open Access (US$4,200)
Please indicate the **city, state/province, and country** where this article will be **filmed**. Please do not use abbreviations.	Wroclaw, Poland
Please confirm that you have read and agree to the terms and conditions of the author license agreement that applies below:	I agree to the Author License Agreement
Please specify the section of the submitted manuscript.	Biochemistry
Please provide any comments to the journal here.	

TITLE:
Spot Variation Fluorescence Correlation Spectroscopy for Analysis of Molecular Diffusion at the Plasma Membrane of Living Cells

AUTHORS AND AFFILIATIONS:
Sébastien Mailfert[1*], Karolina Wojtowicz[2*], Sophie Brustlein[1*], Ewa Blaszczak[3], Nicolas Bertaux[4], Marcin Łukaszewicz[2#], Didier Marguet[1#], Tomasz Trombik[2#]

[1]Aix Marseille Univ, CNRS, Inserm, Centre d'Immunologie de Marseille-Luminy, Turing Center for Living Systems, Marseille, France
[2] Faculty of Biotechnology, University of Wroclaw, Wroclaw, Poland
[3] Faculty of Biological Sciences, University of Wroclaw, Wroclaw, Poland
[4] Aix Marseille Univ, CNRS, Centrale Marseille, Institut Fresnel, Marseille, France

*,# These authors contributed equally.

Email addresses of co-authors:
Sébastien Mailfert (mailfert@ciml.univ-mrs.fr)
Karolina Wojtowicz (karolina.wojtowicz@uwr.edu.pl)
Sophie Brustlein (sophie.brustlein@univ-amu.fr)
Ewa Blaszczak (ewa.blaszczak@uwr.edu.pl)
Nicolas Bertaux (nicolas.bertaux@centrale-marseille.fr)

Co-corresponding authors:
Marcin Łukaszewicz (marcin.lukaszewicz@uwr.edu.pl)
Didier Marguet (marguet@ciml.univ-mrs.fr)
Tomasz Trombik (tomasz.trombik@uwr.edu.pl)

KEYWORDS:
spot variation Fluorescence Correlation Spectroscopy (svFCS), lateral diffusion, plasma membrane dynamics, molecular confinement, lipid nanodomains, cytoskeleton meshwork, diffusion law

SUMMARY:
This article aims to present a protocol on how to build a spot variation Fluorescence Correlation Spectroscopy (svFCS) microscope to measure molecular diffusion at the plasma membrane of living cells.

ABSTRACT:
Dynamic biological processes in living cells, including those associated with plasma membrane organization, occur on various spatial and temporal scales, ranging from nanometers to micrometers and microseconds to minutes, respectively. Such a broad range of biological processes challenges conventional microscopy approaches. Here, we detail the procedure for implementing spot variation Fluorescence Correlation Spectroscopy (svFCS) measurements using

a classical fluorescence microscope that has been customized. The protocol includes a specific performance check of the svFCS setup and the guidelines for molecular diffusion measurements by svFCS on the plasma membrane of living cells under physiological conditions. Additionally, we provide a procedure for disrupting plasma membrane raft nanodomains by cholesterol oxidase treatment and demonstrate how these changes in the lateral organization of the plasma membrane might be revealed by svFCS analysis. In conclusion, this fluorescence-based method can provide unprecedented details on the lateral organization of the plasma membrane with the appropriate spatial and temporal resolution.

INTRODUCTION:

The complexity of plasma membrane organization

The current understanding of cell membrane organization has to take into account several aspects[1]. First, a complex lipid composition varies not only between cell types, but also within a single cell (membrane organelles/plasma membrane). Besides, associated or intrinsic membrane proteins are mostly organized in dynamic multimeric complexes, with large domains extending outside of the membrane, accounting for a significantly larger area than that of the transmembrane domains alone. Moreover, membrane-associated proteins exhibit specific lipid-binding or lipid-interacting capacities that play roles in regulating protein function. These depend directly on the local composition and accessibility of the lipids[2].

Finally, a significant level of asymmetry is observed between two membrane leaflets due to the intrinsic asymmetric structure of membrane proteins and the distribution of lipids. Indeed, a lipid metabolic balance between synthesis and hydrolysis, combined with lipid flip-flop between the leaflets, generates such asymmetric distribution. As any transport across the bilayer is constrained by the free energy required to move the polar head group through the hydrophobic interior of the membranes, it is usually assisted by selective transporters. For each cell type, asymmetry tends to be firmly maintained. Altogether, these factors contribute to lateral inhomogeneity or compartmentalization of the plasma membrane[3,4].

We enrich this representation of the plasma membrane by taking into account the intrinsic molecular diffusion within and across the bilayer, which contributes to the dynamic lateral heterogeneity on a scale of tenths to hundreds of nanometers and microseconds to seconds. For instance, lipid-dependent membrane nanodomains—the so-called lipid rafts, defined as cholesterol, and sphingolipid-rich signaling platforms—contribute to the compartmentalization of the plasma membrane[5,6]. However, the current view of membrane organization is not restricted to lipid rafts alone. Membrane nanodomains are more complex and heterogeneous in composition, origin, and function. Still, their presence at the plasma membrane has to be tightly coordinated, and dynamic interactions between proteins and lipids seem to be important in the spatial distribution and chemical modification of membrane nanodomains[1,3,7,8].

The svFCS principle and its application to probe the organization of the plasma membrane

Although much progress has been made in the analysis of membrane domains, mainly through biophysical techniques, the determinants that dictate the local organization of the plasma

membrane need to be refined with appropriate spatial and temporal resolution. Determinants based on tracking individual molecules provide excellent spatial precision and allow the characterization of different modes of motion[9–12], but have a limited temporal resolution with classical low camera frame rates and require more experimental effort to record a significant number of trajectories. Alternatively, the diffusion coefficient of membrane components can be evaluated by Fluorescence Recovery After Photobleaching (FRAP)[13] or Fluorescence Correlation Spectroscopy (FCS)[14]. The latter has received more attention, mainly because of its high sensitivity and selectivity, microscopic detection volume, low invasiveness, and wide dynamic range[15].

The conceptual basis of FCS was introduced by Magde and colleagues about 50 years ago[16,17]. It is based on recording the fluctuation of fluorescence emission with a high temporal resolution (from µs to s)[18]. In its modern version, measurements in living cells are performed by a small confocal excitation volume (~0.3 femtoliters) positioned within a region of interest (e.g., at the plasma membrane); the fluorescence signal generated by diffusing fluorescent molecules going in and out of the observation volume is collected with very high temporal resolution (i.e., the time of arrival of each photon on the detector). Then, the signal is computed to generate the autocorrelation function (ACF), from which the average time t_d (diffusion time) for which a molecule stays within the focal volume is extracted, together with the mean number of particles, (N), present in the observation volume, which is inversely proportional to the amplitude of the ACF. This last parameter might be useful information on the molecule concentration within the observation volume.

Since then, a growing number of FCS modalities have been implemented thanks to rapidly developing instrumentation in biophotonics, allowing the description of dynamic phenomena occurring in living systems. Still, a molecular species would experience a more overlapping distribution of the diffusion coefficient values, which is usually reflected by an anomalous diffusion characteristic, in which molecules diffuse with a nonlinear relationship in time[19], and difficulty in identifying the biological meaning of this anomalous subdiffusion. In the past, this difficulty has been somewhat overcome by recording the molecular diffusion by FRAP from areas of various sizes, rather than from just one area, thereby providing additional spatial information. This enabled, for instance, the conceptualization of membrane microdomains[20–22].

A translation of this strategy to FCS measurements (i.e., the so-called spot variation Fluorescence Correlation Spectroscopy (svFCS)) was established by varying the size of the focal volume of observation, allowing the fluctuation in fluorescence to be recorded on different spatial scales[23]. Thus, the svFCS approach provides indirect spatial information allowing for the identification and determination of molecular diffusion modes and type of membrane partitioning (isolated versus contiguous domains[24]) of studied molecules. By plotting the diffusion time t_d as a function of the various spatial scales defined by the waist ω value, which corresponds to the detection beam radius size here[23, 25], one can characterize the diffusion law of a given molecule in a given physiological condition. The svFCS is, therefore, a perfect analog to single-particle tracking in the time domain[26]. Under the Brownian diffusion constraint, one should expect a strictly linear relationship between the time t_d and the waist ω (**Figure 1**)[23,25]. The origin of the deviation of the

diffusion law from this scheme can be attributed to nonexclusive reasons, such as cytoskeleton meshwork, molecular crowding, dynamic partitioning in nanodomains, or any combination of these and other effects (**Figure 1**), and needs to be tested experimentally[25].

Here we provide all necessary control checkpoints for the daily use of a custom-made svFCS optical system built from scratch, which complements our previous protocol reviews[27,28] on that experimental approach. Further, as a proof of concept, we give guidelines regarding the calibration of the setup, the preparation of cells, data acquisition, and analysis for the establishment of svFCS diffusion law (DL) for Thy1-GFP, a plasma membrane glycosylphosphatidylinositol-anchored protein, which is known to be localized in lipid-raft nanodomains[29]. Finally, we demonstrate how the partial destabilization of lipid-raft nanodomains by cholesterol oxidase treatment impacts the diffusion properties of Thy1-GFP. Additionally, a detailed description of building a svFCS setup from scratch is provided in **Supplementary Material**.

PROTOCOL:

1. Setting specification for assembling a custom-made svFCS setup

NOTE: The simplicity of the proposed svFCS setup allows easy installation, operation, and maintenance at a low cost while ensuring efficiency in photon recovery. For more details, see **Supplementary material**.

1.1. Experimental room and safety

1.1.1. Install the system in a room stabilized at around 21 °C.

1.1.2. Avoid direct airflow on the passive (or active) optical table and follow the laser safety rules for optical alignment.

1.2. Hardware and software

NOTE: **Supplementary Material** details the installation steps depicted in **Figure 2**.

1.2.1. Write the main acquisition and control software in LabVIEW using a state machine and event structure architecture where a multifunction acquisition board drives most of the controllers.

NOTE: The correlator, laser, and power meter are controlled or monitored by their own software.

1.2.2. Adapt the hardware and software installation procedures according to the hardware used.

1.3. Optical setup

NOTE: **Figure 3** illustrates the optical bench modules used in the following sections to control the quality of the optical alignments. All of the optical element specifications are listed in **Table of materials**. The procedure to build the setup is widely detailed in **Supplementary Material**. This system comprises a continuous wave laser, a motorized inverted microscope equipped with an immersion water objective, an avalanche photodiode detector coupled to a single photon counting module, and a hardware correlator. A microscope incubation chamber with vibration-free heaters has been specially designed to control the temperature for experiments on living cells. By convention, the XY axis corresponds to the optical path's perpendicular plane, and the Z-axis corresponds to the optical path.

2. Daily checkpoint before running the experiment

2.1. Control the excitation path (**Figure 3**, ① & ②).

2.1.1. Open all the iris diaphragms.

2.1.2. Measure the laser power with the power meter, keeping the first iris fully open.

2.1.3. Turn the half-wave plate (HWP) to find the maximum power.

2.1.4. Check the alignment using the irises if the laser power is lower than usual, and move L1 and M1 alternately, if necessary.

2.1.5. Note the power value in the experiment laboratory notebook.

2.2. Control the detection path (**Figure 3**, ③ & ④).

2.2.1. Place the water, a coverslip, and a droplet of a 2 nM rhodamine 6G (Rh6G) solution on the objective.

2.2.2. If the fluorescence signal (count number on the APD, recorded with the LabVIEW software) is lower than usual, remake the Rh6G solution, check the positioning and the coverslip's number on the objective lens, or eliminate bubbles, if any.

2.2.2.1. If the fluorescence signal is still lower than usual, place the power meter inside the optical path to block the beam.

2.2.2.2. Turn off the APD (hereafter, APD refers to the APD and the single photon counting module).

2.2.2.3. Remove the sample.

2.2.2.4. Clean and replace the objective lens with a reflective target.

2.2.2.5. Check the laser beam on the reflective target by removing the power meter from the light path. Make sure that the target's beam is centered, and the back reflection reaches the first iris on the line ② (**Figure 3**).

2.2.2.6. If not, adjust the center positioning with M2 or the back reflection with the dichroic mirror.

2.2.2.7. If microscope coupling is correct, push the objective lens back, add a drop of water, a coverslip, and a droplet of a more concentrated Rh6G solution (i.e., 200 nM), and set a lower laser power than for the classical measurements (few µW).

2.2.2.8. Turn on the APD and optimize APD and pinhole alignment, alternately, with their respective XYZ adjustment screws while monitoring the intensity signal (LabVIEW software).

2.2.2.9. Change the coverslip and add a lower concentration of Rh6G (2 nM). Move the pinhole along the Z-axis to find a position where the molecular brightness ratio increases, and the waist is minimum.

2.2.2.10. Close the iris until the signal drops down: the laser beam size reaches the back aperture size of the objective (i.e., the minimal waist size, see **Supplementary material**).

2.2.2.11. Launch the correlator software and record data (see section 7 for data recording).

2.2.2.12. Check the ACF, which should display a low amount of noise, give a small waist size, and a high count-rate per molecule per second (see section 7 for data analysis and waist size evaluation).

3. General considerations for svFCS data recording and analysis

3.1. Record and analyze the fluorescence data following this general scheme (see sections 7, 8, and 9): (1) fluorescence recording and ACF generation (correlator software), (2) unexpected discarding of data, an average of retained data, fitting with the appropriate model (with homemade Igor Pro software), (3) diffusion law plot (homemade MATLAB software 1), and (4) optional diffusion law comparison (homemade MATLAB software 2). The different software programs are available upon request.

NOTE: The hardware correlator has a minimum sampling time of 12.5 ns (i.e., a sampling frequency of 80 MHz). It provides a temporal resolution that is at least 1,000 lower than the typical resident time of freely diffusing small molecule in solution and 10^6 smaller than the diffusion time of membrane proteins within a confocal observation volume.

4. Cell culture and transfection

4.1. Seed the Cos7 cells in 8-well chambered coverglass with #1.0 borosilicate glass bottom at a density of 10,000 cells/well using complete Dulbecco's Modified Eagle Medium (DMEM) supplemented with 5% fetal bovine serum, penicillin (100 U/mL), streptomycin (100 U/mL), and L-glutamine (1 mM).

4.2. Culture the cells at 37 °C in a humidified atmosphere containing 5% CO_2 for 24 h.

4.3. Remove the medium, add 300 µL of the fresh complete culture medium per well, and preincubate the cells for 30 min at 37 °C.

4.4. Dilute 0.5 µg of the plasmid DNA encoding Thy-1 protein fused with eGFP[25] in 50 µL of serum-free DMEM. Vortex briefly to mix.

4.5. Dilute1.5 µL of the DNA transfection reagent in 50 µL of serum-free DMEM, and mix the solution well.

4.6. Add the diluted transfection reagent directly into the prepared DNA solution, and mix the compounds immediately.

4.7. Incubate the prepared mixture for 10 to 15 min at room temperature.

4.8. Add 10 µL of the combined DNA/transfection reagent complexes dropwise onto the medium in each well, and homogenize by gently swirling the plate.

4.9. Incubate the cells at 37 °C with 5% CO_2 for 3 h.

4.10. After the incubation, replace the medium containing DNA/transfection reagent complexes with 400 µL of fresh complete DMEM, and culture the cells for 16 h before the svFCS experiment.

5. Preparation of cells for svFCS measurements

5.1. Remove the culture medium.

5.2. Wash the cells gently two to three times with serum-free Hank's balanced salt solution (HBSS) buffer containing Ca^{2+} and Mg^{2+} supplemented with 10 mM (4-(2-hydroxyethyl)-1-piperazineethanesulfonic acid) (HEPES), pH 7.4 (HBSS/HEPES).

5.3. Maintain the cells in HBSS/HEPES buffer during all svFCS acquisitions.

6. Pharmacological treatment

6.1. Remove the culture medium, and wash the cells two to three times with serum-free HBSS supplemented with 10 mM HEPES, pH 7.4 (HBSS/HEPES).

6.2. Incubate the cells with 1 U/mL of cholesterol oxidase (COase) solution in HBSS/HEPES buffer for 1 h at 37 °C.

6.3. Remove the solution, and maintain the cells in the presence of 0.1 U/mL of COase in HBSS/HEPES buffer while performing the svFCS measurements.

7. Spot size calibration

7.1. Prewarm the microscope chamber at 37 °C.

7.2. Prepare a standard 2 nM solution of Rh6G by serial dilution.

7.3. Drop 200 µL of 2 nM Rh6G solution on a glass coverslip placed on the water-immersion objective.

7.4. Start all the hardware and software.

7.5. Measure and adjust the 488 nm laser beam power to 300 µW.

7.5.1. Depending on the brightness and the photo-stability of the fluorescent probe used, adapt this power according to (1) the fluorescence intensity (on the LabVIEW software), which should be stable, (2) the ACF shape (on the correlator software), which should have a constant shape over the time, and (3) the fitting parameters giving a small waist size and a high count rate per molecule (photons per molecule per second, typically few tens to hundreds of photons per molecule per second).

NOTE: The amplitude of the ACF (called G(0)) is inversely proportional to the number of the molecule (i.e., the concentration of the fluorescent probe). For the waist size calibration, this is a good quality control candidate parameter. Therefore, G(0) should be similar for the same concentration from day to day as it links the waist size and concentration. For cell measurements, as FCS is more accurate for low concentration, G(0) should be high for the proper parameter fitting extraction.

7.6. Set the svFCS illumination/detection microscope port with the LabVIEW software.

7.7. Turn on the APD.

7.8. Close the iris until the signal drops down to obtain the minimal waist size, or close it for bigger waist size.

7.9. Record several ACFs of selected duration (namely a run) to improve statistical

reproducibility, typically 10 runs lasting for 20 s each with the correlator software.

7.10. Turn off the APD.

7.11. Use the Igor Pro software to check and discard the runs with strong fluctuations due to molecular aggregates. Perform this step manually— it should be user-independent after users have been trained.

7.12. Fit the average of the retained ACFs with a 3D diffusion model.

7.13. Extract from the fitting parameters the average diffusion time τ_D and save it into a ".txt" file (the file format is dictated by the Igor Pro software).

7.14. Check the count-rate per molecule per second (a good performance indicator) by dividing the average intensity (extracted from the fluorescence trace) by the number of molecules (extracted from the ACF).

NOTE: Make sure that this value is high and stable from day to day for the same acquisition parameters.

7.15. Knowing the diffusion coefficient of Rh6G in aqueous solution at 37 °C (D) and τ_D(see 7.13), calculate the experimental waist size ω according to : $\omega = \sqrt{4 \times \tau_D \times D}$.

7.16. Apply the procedure for every waist size modification required to plot the FCS diffusion law and before any new experimental series of svFCS data acquisition.

8. svFCS data acquisitions on cells

8.1. Measure and adjust the 488 nm beam power between 2 and 4 µW. Depending on the brightness and the photostability of the fluorescent probe used, adapt this power to allow a high count rate per molecule (typically several thousand of photons per molecule per second), while keeping the photobleaching low (i.e., a stable intensity trace on the LabVIEW software).

8.2. Equilibrate samples for 10 min at 37 °C before starting the measurements.

8.3. Set the epi-fluorescence illumination microscope with the LabVIEW software.

8.4. Choose a cell with an appropriate fluorescent probe location and (low) fluorescence signal intensity.

NOTE: The lower the fluorescence is, the better the FCS measurements are (see step 8.1).

8.5. Set the svFCS illumination/detection microscope port with the LabVIEW software.

8.6. Turn on the APD.

8.7. Perform an xy-scan of the selected cell with the LabVIEW software.

8.8. Perform a z-scan and locate the confocal spot at the maximal fluorescence intensity by choosing the plasma membrane at the top and start the data acquisition. To maximize the separation between the two membranes, preferably perform the scan in the nuclear area of the cell.

8.9. Record one series of 20 runs lasting for 5 s, each with the correlator software.

NOTE: Make sure that the duration of each run is long enough to obtain ACFs with reduced noise. Long acquisitions are susceptible to photobleaching or unexpected substantial variations (e.g., aggregates). Adapt the number of runs, their duration, and the number of series to the samples, but make sure that they remain constant within the same bulk of experiments for reproducibility.

8.10. Turn off the APD.

8.11. Discard unexpected runs with the Igor Pro software.

8.12. Fit the average ACF with a 2-species 2D diffusion model. Adapt this model to the type of diffusion behavior of the target molecule.

8.13. Save the fitting parameters into the previous file (see step 7.13).

8.14. Perform 10 to 15 series of recordings on at least 10 different cells, and reproduce steps 8.3 to 8.13. Check that the single file obtained contains the waist size information and the fitting parameters of the 10–15 recordings.

8.15. To establish a single diffusion law, analyze at least four waist sizes varying between 200 and 400 nm. This range is defined by the diffraction optical limit, but is objective- (numerical aperture) and laser (wavelength)-dependent.

NOTE: As the waist size calibration is not absolute and has some degree of uncertainty, a dedicated MATLAB software[28] accounting for the x and y error (namely ω^2 and t_d) was built to fit the diffusion law.

8.16. Start the MATLAB software 1 and select a folder containing all the ".txt" files corresponding to at least four waist size experiments.

8.17. Plot $<t_d>$ versus $<\omega^2>$, namely the diffusion law. Two major parameters can be extracted: the y-axis intercept (t_0) and the effective diffusion coefficient (D_{eff}, inversely proportional to the slope).

9. Diffusion laws of different experimental condition comparison

NOTE: If necessary, reproduce sections 7 and 8 for different experimental conditions. A dedicated software (MATLAB software 2) was developed to determine whether these diffusion laws are similar or not according to the t_0 and D_{eff} values[28]. It tests two hypotheses: the two values are different, or the two values are not different at a threshold set above a probability of false alarm (PFA). An arbitrary PFA value of 5% (T = 3.8) is considered the upper limit of significance between two parameters (t_0 or D_{eff}), indicating that there is only 5% chance that the two values are identical.

9.1. Create an ".xls" file containing the characteristic diffusion law values of each condition to compare (i.e., a file containing the t_0, t_0 error, D_{eff} and D_{eff} error for the non-treated (NT) and treated (COase) conditions as a table).

9.1.1. Start the MATLAB software 2.

9.1.2. Select the ".xls" file.

9.1.3. Analyze the generated color-coded 2D plot, where the t_0 and D_{eff} statistical tests are to be plotted on the x- and y-axes, respectively (**Figure 4**). The higher T is, the greater is the difference between the compared values.

10. Cholesterol concentration measurements

10.1. Cell treatment and lysis

10.1.1. Seed the Cos7 cells in triplicate in 6-well plates at 4×10^5 cells/well and incubate in 2 mL of complete DMEM at 37 °C with 5% CO_2 overnight to allow the cells to attach to the plate.

10.1.2. Remove the culture medium and wash the cells three times with phosphate-buffered saline (PBS).

10.1.3. Add 1 mL of HBSS/HEPES buffer containing (or not, for controls) 1 U/mL of Coase, and incubate for 1 h at 37 °C with 5% CO_2.

10.1.4. Replace the medium with 1 mL of HBSS/HEPES containing 0.1 U/mL of Coase, and incubate for 1 h at 37 °C with 5% CO_2.

10.1.5. Remove the solution and harvest the cells.

10.1.6. Wash the cells three times with PBS, and centrifuge at 400 × *g* for 5 min at room temperature.

10.1.7. Lyse the cells with radioimmunoprecipitation assay buffer (25 mM HEPES, pH 7.4, 150 mM NaCl, 1% NP40, 10 mM, $MgCl_2$, 1 mM ethylenediamine tetraacetic acid, 2% glycerol, protease and phosphatase inhibitor cocktail) for 30 min on ice.

10.1.8. Centrifuge the lysates at 10000 × *g* for 10 min at 4 °C and collect the supernatant.

10.2. Quantify total protein concentration for each sample by modified Bradford's protein assay using the working solution according to the manufacturer's recommendations.

10.3. Cholesterol concentration measurement

10.3.1. To determine total cellular cholesterol level enzymatically, use the appropriate kit (e.g., Amplex Red Cholesterol Assay Kit) according to the manufacturer's recommendations.

10.3.2. For each reaction, mix the sample containing 5 µg of protein with Amplex Red reagent/horseradish peroxidase/cholesterol oxidase/cholesterol esterase working solution, and incubate for 30 min at 37 °C in the dark.

10.3.3. Measure the fluorescence using excitation of 520 nm, and detect the emission at 560–590 nm using a microplate reader.

10.3.4. Subtract the background from the final value, and determine cholesterol concentration using a standard curve.

10.3.5. Calculate the final cholesterol content in ng of cholesterol per µg of protein.

REPRESENTATIVE RESULTS:

We generated a DL for Thy1-GFP expressed in Cos-7 cells (**Figure 4**, black squares). The diffusion law has a positive t_0 value (19.47 ms ± 2 ms), indicating that Thy1-GFP is confined in nanodomain structures of the plasma membrane. The cholesterol oxidase treatment of the cells expressing Thy1-GFP resulted in the shift of the DL t_0 value to 7.36 ± 1.34 ms (**Figure 4**, gray squares). This observation confirms that the nature of Thy1-GFP confinement depends on the cholesterol content and is associated with lipid raft nanodomains. These two diffusion laws are shown to be different according to the statistical test described above (see step 9.1.3) in terms of t_0 and D_{eff} values. In addition, we assessed the concentration of total cellular cholesterol in non-treated Cos-7 cells versus the cells treated with COase. A small, but significant, decrease in total cholesterol content is observed upon COase treatment (**Figure 5**). As this enzyme acts only on the cholesterol pool accessible at the outer leaflet of the plasma membrane, we assume that the observed decrease in cholesterol is associated only with the plasma membrane and results in the destabilization of lipid raft nanodomains.

FIGURE AND TABLE LEGENDS:

Figure 1: Simulated fluorescence correlation spectroscopy (FCS) diffusion laws established by spot-variation FCS for different forms of membrane organization. (Upper panels) Schematic representation of membrane organization—(**A**) free diffusion, (**B**) meshwork barriers, and (**C**) trap/domain confinements—with the trajectory drawn for a single molecule (red). Blue circles denote the intersection of the membrane and laser beam of waist ω. (Lower panels) FCS diffusion laws represented by plotting the diffusion time t_d as a function of the squared radius ω^2. Diffusion law projection (green dashed line) intercepts the time axis at (**A**) the origin ($t_0 = 0$) in the case of free diffusion; (**B**) in negative axis ($t_0 < 0$) when there are meshwork barriers, or (**C**) in positive axis ($t_0 > 0$) when there are traps and domains (lipid rafts). D is the lateral diffusion coefficient for Brownian motion; D_{eff}, the effective diffusion coefficient; D_{micro}, the microscopic diffusion coefficient inside the meshwork traps; D_{in}, the diffusion coefficient inside domains; D_{out}, the diffusion coefficient outside domains; L, the size of the side of a square domain; and r_D, the radius of a circular domain. This figure has been modified from He and Marguet[6].

Figure 2: Schematic view of svFCS hardware control. The computer controls all the devices through different communication protocols: serial (microscope, external shutter), USB (XYZ piezoelectric stage, correlator), and PCI (acquisition board). DAQ: data acquisition board, APD: avalanche photodiode, SPCM: single-photon counting module, DO: digital output.

Figure 3: **Schematic view of excitation and emission optical paths of the svFCS setup.** The svFCS setup contains four modules: (1) the output of a fibered 488 nm laser is collimated, (2) a combination of a half-wave plate and polarizing beam-splitter sets the optical power, (3) the laser beam focused on the sample after traveling through a tube-lens free motorized microscope, and (4) the fluorescence is detected through a confocal-like detection path onto an avalanche photodiode coupled to a single photon counting module, which delivers a signal to a hardware correlator. Simplicity gives the system its sensitivity, robustness, and ease of use (widely commented in **Supplementary material**).

Figure 4: The svFCS diffusion laws generated from diffusion analysis of Thy1-GFP expressed in Cos-7. svFCS diffusion laws of Cos-7 cells without treatment (NT, black squares) and after cholesterol oxidase treatment (COase, gray circles). The insert in the graph represents statistical testing of a significant difference between the two presented svFCS diffusion laws (according to Mailfert et al.[28]). The test value (T) should be above the threshold set at 3.8 when both diffusion laws are different. The higher it is, the greater is the difference between the diffusion laws. The value of T is color-coded.

Figure 5: Comparison of total cholesterol content in Cos-7 cells. Cos-7 cells were either non-treated (NT) or treated with 1 U/mL of cholesterol oxidase (COase) for 1 h. The data represent an example of one experiment in triplicate. A two-tailed, unpaired *t*-test was used to assess the statistical difference (α=0.05).

Table of materials: The list of optical elements required for the svFCS setup.

Supplementary material: This document describes the building of a svFCS setup from scratch.

DISCUSSION:

Here, we have described the implementation of the svFCS module on a standard fluorescent microscope, a powerful experimental approach to decipher the dynamics of the plasma membrane organization in living cells thanks to the FCS diffusion law analysis. Conceptually, the svFCS is based on a simple principle: correlation measurements of fluorescence in the time domain while varying the size of the illumination area[23]. This strategy has been instrumental in deducing nanoscopic information from microscopic measurements, which helps decipher the main physicochemical elements contributing to the plasma membrane organization in steady state[25] and physiological processes[30–33]. Altogether, these svFCS analyses unambiguously demonstrate the existence of lipid-dependent nanodomains in various cell types and their direct implication in tuning different signaling events.

Within this framework, there are some optical aspects that need to be considered while building the svFCS setup to optimize the photon budget and minimize optical aberrations. Thus, we recommend using a microscope from which the tube lens can be removed when the svFCS measurement is performed. Moreover, a single iris plays a key role in the svFCS setup: it changes the beam size at the back aperture of the objective, thus directly varying the effective waist size (i.e., the effective excitation volume). The beam diameter should fit the objective back pupil to obtain the smallest waist size[34]. This option, which helps tune the waist size, ensures optimization of the photon budget and is easy to implement. Finally, a minimal number of optical parts are used along the light path; the less complex the system, the fewer the photons that are lost. All of these options significantly improve the robustness of svFCS experiments.

Regarding the protocol itself, a few critical steps have to be considered. The most important is an appropriate alignment of the optical paths that is crucial for successful svFCS measurements (protocol, section 2). This is easy to check by analyzing the fluorescence signal from a 2 nM Rh6G solution, which should be ~200 kHz under 300 µW laser illumination. All irises should be opened, and the ACFs should have an important amplitude (typically G0~1.5–2.0). Another critical point concerns the cells and their preparation for svFCS analysis (protocol, sections 4–8). Their density has to be adapted so that isolated cells to be observed are available for analysis. Non-adherent cells have to be immobilized on a chambered coverglass by using poly-L-lysine solution. The fluorescence signal from cell labeling should not be too strong, or it will result in very flat ACFs that are difficult to fit, and the fit parameters are burdened with an important error. Additionally, nonhomogeneous labeling and fluorescence aggregates in cells make the svFCS measurements extremely difficult to interpret. Finally, cholesterol oxidase treatment affects cell viability, and the svFCS analysis should not exceed one hour after the treatment. It is also better to record the fluorescence fluctuations from the upper plasma membrane as it is not attached to the support, and there is no risk of hindered diffusion of molecules due to the physical interactions with the support.

There have been enough advances in the svFCS technique for its use in different approaches owing to the diversity of modalities for adjusting the detection volume, making it possible to study various biological processes in living cells. An alternative to adjusting the size of the

excitation volume is to use a variable beam expander[35]. It is also possible to simply modulate the size of the illumination area by recording the fluorescent signal from the intercept of the plasma membrane along the z direction[36]. This can be done on a standard confocal microscope for which a theoretical framework has been developed to derive the diffusion law[37,38].

Although the svFCS method offers spatio-temporal resolution, which is necessary for the characterization of the inhomogeneous lateral organization of the plasma membrane, the geometrical modes of confinement are not mutually exclusive. A deviation of t_0 in one direction or the other exclusively reveals a dominant mode of confinement[25]. Moreover, another important limitation of the present svFCS method results from the classical optical diffraction limit (~200 nm). This is unquestionably greater than the domains confining the molecules within the cell plasma membrane. Therefore, the analysis of the confinement is inferred from the t_0 value, extrapolated from the diffusion law.

This drawback has been overcome by implementing alternative methods. Initially, using metallic films drilled with nanoapertures offered the possibility of illuminating a very small membrane area (i.e., below the optical diffraction limit of single nanometric apertures of radii varying between 75 and 250 nm)[39]. The transition regime predicted from the theoretical diffusion law for isolated domain organization was thus reported, and it allowed a refinement of the characteristic size of the nanometric membrane heterogeneities and a quantitative estimate of the surface area occupied by lipid-dependent nanodomains[39]. Alternatively, nanometric illumination has also been developed using near-field scanning optical microscopy[40] or planar optical nanoantennas[41]. More recently, combining stimulated emission depletion (STED) and FCS has provided a powerful and sensitive tool to document the diffusion law with very high spatial resolution. This STED-FCS gives access to molecular diffusion characteristics on a nanoscale occurring within a short period of time, allowing the study of the dynamic organization of lipid probes at the plasma membrane[42,43]. However, the incomplete suppression of fluorescence in the STED process challenges the analysis of the auto-correlation curves in FCS.

A new fitting model has been developed to overcome this difficulty, improving the accuracy of the diffusion times and average molecule numbers measurements[44]. Finally, for slow molecular diffusion at the plasma membrane, the svFCS principle can be applied to data recorded by image correlation spectroscopy[45]. Recently, it has been demonstrated that combining atomic force microscopy (AFM) with imaging total internal reflection-FCS (ITIR-FCS) contributes to the refinement of the nature of the mechanism hindering molecular diffusion at the plasma membrane, especially near the percolation threshold membrane configuration because of a high density of nanodomains[46].

In conclusion, establishing diffusion law by svFCS has provided the experimental evidence to infer local heterogeneity created by dynamic collective lipids and membrane proteins' associations. As stated by Wohland and co-workers[46], "the FCS diffusion law analysis remains a valuable tool to infer structural and organizational features below the resolution limit from dynamic information". Still, we need to develop new models to refine the interpretation of the diffusion law that should allow for a better understanding of the dynamics of the molecular events

occurring at the plasma membrane.

ACKNOWLEDGMENTS:

SB, SM and DM was supported by institutional funding from the CNRS, Inserm and Aix-Marseille University and program grants from the French National Research Agency (ANR-17-CE15-0032-01 and ANR-18-CE15-0021-02) and the French "Investissement d'Avenir" (ANR-10-INBS-04 France-BioImaging, ANR-11-LABX-054 labex INFORM). KW acknowledges "BioTechNan", a program of interdisciplinary environmental doctoral studies KNOW in the field of Biotechnology and Nanotechnology. EB acknowledges the financial support of the National Science Centre of Poland (NCN) under project no. 2016/21/D/NZ1/00285, as well as the French Government and the Embassy of France in Poland. MŁ acknowledges the financial support from the Polish Ministry of Development (CBR POIR.02.01.00-00-0159/15-00/19) and the National Center for Research and Development (Innochem POIR.01.02.00-00-0064/17). TT acknowledges financial support from the National Science Center of Poland (NCN) under project no. 2016/21/B/NZ3/00343 and from the Wroclaw Biotechnology Center (KNOW).

DISCLOSURES:

The authors have nothing to disclose.

REFERENCES:

1. Engelman, D. M. Membranes are more mosaic than fluid. *Nature*. **438** (7068), 578–580, doi: 10.1038/nature04394 (2005).
2. Newton, A. C. Regulation of the ABC kinases by phosphorylation: protein kinase C as a paradigm. *The Biochemical Journal*. **370** (Pt 2), 361–371, doi: 10.1042/BJ20021626 (2003).
3. Marguet, D., Lenne, P. F., Rigneault, H., He, H. T. Dynamics in the plasma membrane: how to combine fluidity and order. *The EMBO Journal*. **25** (15), 3446–3457, doi: 10.1038/sj.emboj.7601204 (2006).
4. Edidin, M. The state of lipid rafts: From model membranes to cells. *Annual Review of Biophysics and Biomolecular Structure*. doi: 10.1146/annurev.biophys.32.110601.142439 (2003).
5. Lingwood, D., Simons, K. Lipid rafts as a membrane-organizing principle. *Science*. doi: 10.1126/science.1174621 (2010).
6. He, H. T., Marguet, D. Detecting nanodomains in living cell membrane by fluorescence correlation spectroscopy. *Annual Reviews of Physical Chemistry* **62**, 417–436, doi: 10.1146/annurev-physchem-032210-103402 (2011).
7. Rossy, J., Ma, Y., Gaus, K. The organisation of the cell membrane: Do proteins rule lipids? *Current Opinion in Chemical Biology*. **20** (1), 54–59, doi: 10.1016/j.cbpa.2014.04.009 (2014).
8. Nicolson, G. L. The Fluid - Mosaic Model of Membrane Structure: Still relevant to understanding the structure, function and dynamics of biological membranes after more than 40 years. *Biochimica et Biophysica Acta - Biomembranes*. **1838** (6), 1451–1466, doi: 10.1016/j.bbamem.2013.10.019 (2014).
9. Fujiwara, T., Ritchie, K., Murakoshi, H., Jacobson, K., Kusumi, A. Phospholipids undergo hop diffusion in compartmentalized cell membrane. *The Journal of Cell Biology*. **157** (6), 1071–1081, doi: 10.1083/jcb.200202050 (2002).
10. Kusumi, A. et al. Paradigm shift of the plasma membrane concept from the two-

dimensional continuum fluid to the partitioned fluid: high-speed single-molecule tracking of membrane molecules. *Annual Review of Biophysics and Biomolecular Structure*. **34**, 351–378, doi: 10.1146/annurev.biophys.34.040204.144637 (2005).
11. Destainville, N., Salomé, L. Quantification and correction of systematic errors due to detector time-averaging in single-molecule tracking experiments. *Biophysical Journal*. **90** (2), L17-L19, doi: 10.1529/biophysj.105.075176 (2006).
12. Wieser, S., Moertelmaier, M., Fuertbauer, E., Stockinger, H., Schütz, G. J. (Un)confined diffusion of CD59 in the plasma membrane determined by high-resolution single molecule microscopy. *Biophysical Journal*. **92** (10), 3719–3728, doi: 10.1529/biophysj.106.095398 (2007).
13. Axelrod, D., Koppel, D. E., Schlessinger, J., Elson, E., Webb, W. W. Mobility measurement by analysis of fluorescence photobleaching recovery kinetics. *Biophysical Journal*. doi: 10.1016/S0006-3495(76)85755-4 (1976).
14. Petrášek, Z., Schwille, P. Precise measurement of diffusion coefficients using scanning fluorescence correlation spectroscopy. *Biophysical Journal*. doi: 10.1529/biophysj.107.108811 (2008).
15. Elson, E. L. 40 Years of FCS: How it all began. *Methods in Enzymology*. doi: 10.1016/B978-0-12-388422-0.00001-7 (2013).
16. Elson, E. L., Magde, D. Fluorescence correlation spectroscopy. I. Conceptual basis and theory. *Biopolymers*. doi: 10.1002/bip.1974.360130102 (1974).
17. Magde, D., Elson, E. L., Webb, W. W. Fluorescence correlation spectroscopy. II. An experimental realization. *Biopolymers*. doi: 10.1002/bip.1974.360130103 (1974).
18. Schwille, P., Haupts, U., Maiti, S., Webb, W. W. Molecular dynamics in living cells observed by fluorescence correlation spectroscopy with one- and two-photon excitation. *Biophysical Journal*. doi: 10.1016/S0006-3495(99)77065-7 (1999).
19. Bouchaud, J. P., Georges, A. Anomalous diffusion in disordered media: Statistical mechanisms, models and physical applications. *Physics Reports*. doi: 10.1016/0370-1573(90)90099-N (1990).
20. Yechiel, E., Edidin, M. Micrometer-scale domains in fibroblast plasma membranes. *Journal of Cell Biology* **105** (2), 755–760 (1987).
21. Salomé, L., Cazeils, J. L., Lopez, A., Tocanne, J. F. Characterization of membrane domains by FRAP experiments at variable observation areas. *European Biophysics Journal* **27** (4), 391–402 (1998).
22. Niv, H., Gutman, O., Kloog, Y., Henis, Y. I. Activated K-Ras and H-Ras display different interactions with saturable nonraft sites at the surface of live cells. *The Journal of Cell Biology*. **157** (5), 865–872, doi: 10.1083/jcb.200202009 (2002).
23. Wawrezinieck, L., Rigneault, H., Marguet, D., Lenne, P. F. Fluorescence correlation spectroscopy diffusion laws to probe the submicron cell membrane organization. *Biophysical Journal*. **89** (6), 4029–4042, doi: 10.1529/biophysj.105.067959 (2005).
24. Saxton, M. J. Fluorescence corralation spectroscopy. *Biophysical Journal*. doi: 10.1529/biophysj.105.074161 (2005).
25. Lenne, P. F. et al. Dynamic molecular confinement in the plasma membrane by microdomains and the cytoskeleton meshwork. *EMBO Journal*. **25** (14), 3245–3256, doi: 10.1038/sj.emboj.7601214 (2006).
26. Ruprecht, V. et al. Cortical contractility triggers a stochastic switch to fast amoeboid cell

motility. *Cell*. doi: 10.1016/j.cell.2015.01.008 (2015).
27. Billaudeau, C. et al. Probing the plasma membrane organization in living cells by spot variation fluorescence correlation spectroscopy. *Methods in Enzymology*. **519**, 277–302, doi: 10.1016/B978-0-12-405539-1.00010-5 (2013).
28. Mailfert, S., Hamon, Y., Bertaux, N., He, H. T., Marguet, D. A user's guide for characterizing plasma membrane subdomains in living cells by spot variation fluorescence correlation spectroscopy. *Methods in Cell Biology*. **139** (January), 1–22, doi: 10.1016/bs.mcb.2016.12.002 (2017).
29. Rege, T. A., Hagood, J. S. Thy-1, a versatile modulator of signaling affecting cellular adhesion, proliferation, survival, and cytokine/growth factor responses. *Biochimica et Biophysica Acta - Molecular Cell Research*. doi: 10.1016/j.bbamcr.2006.08.008 (2006).
30. Cahuzac, N. et al. Fas ligand is localized to membrane rafts, where it displays increased cell death-inducing activity. *Blood*. doi: 10.1182/blood-2005-07-2883 (2006).
31. Guia, S. et al. Confinement of activating receptors at the plasma membrane controls natural killer cell tolerance. *Science Signaling*. **4** (167), ra21 (2011).
32. Blouin, C. M. et al. Glycosylation-dependent IFN-γR partitioning in lipid and actin nanodomains is critical for JAK activation. *Cell*. **166** (4), 920–934, doi: 10.1016/j.cell.2016.07.003 (2016).
33. Chouaki-Benmansour, N. et al. Phosphoinositides regulate the TCR/CD3 complex membrane dynamics and activation. *Scientific Reports*. doi: 10.1038/s41598-018-23109-8 (2018).
34. Wawrezinieck, L., Lenne, P. F., Marguet, D., Rigneault, H. Fluorescence correlation spectroscopy to determine diffusion laws: application to live cell membranes. *Biophotonics Micro- and Nano-Imaging*. doi: 10.1117/12.545014 (2004).
35. Masuda, A., Ushida, K., Okamoto, T. New fluorescence correlation spectroscopy enabling direct observation of spatiotemporal dependence of diffusion constants as an evidence of anomalous transport in extracellular matrices. *Biophysical Journal*. doi: 10.1529/biophysj.104.048009 (2005).
36. Humpolíčková, J. et al. Probing diffusion laws within cellular membranes by Z-scan fluorescence correlation spectroscopy. *Biophysical Journal*. doi: 10.1529/biophysj.106.089474 (2006).
37. Benda, A. et al. How to determine diffusion coefficients in planar phospholipid systems by confocal fluorescence correlation spectroscopy. *Langmuir*. doi: 10.1021/la0270136 (2003).
38. Ganguly, S., Chattopadhyay, A. Cholesterol depletion mimics the effect of cytoskeletal destabilization on membrane dynamics of the serotonin1A receptor: A zFCS study. *Biophysical Journal*. doi: 10.1016/j.bpj.2010.06.031 (2010).
39. Wenger, J. et al. Diffusion analysis within single nanometric apertures reveals the ultrafine cell membrane organization. *Biophysical Journal*. **92** (3), 913–919, doi: 10.1529/biophysj.106.096586 (2007).
40. Manzo, C., Van Zanten, T. S., Garcia-Parajo, M. F. Nanoscale fluorescence correlation spectroscopy on intact living cell membranes with NSOM probes. *Biophysical Journal*. doi: 10.1016/j.bpj.2010.12.3690 (2011).
41. Regmi, R. et al. Planar optical nanoantennas resolve cholesterol-dependent nanoscale heterogeneities in the plasma membrane of living cells. *Nano Letters*. doi: 10.1021/acs.nanolett.7b02973 (2017).

42. Mueller, V. et al. FCS in STED microscopy: Studying the nanoscale of lipid membrane dynamics. *Methods in Enzymology*. doi: 10.1016/B978-0-12-405539-1.00001-4 (2013).
43. Sezgin, E. et al. Measuring nanoscale diffusion dynamics in cellular membranes with super-resolution STED–FCS. *Nature Protocols*. doi: 10.1038/s41596-019-0127-9 (2019).
44. Wang, R. et al. A straightforward STED-background corrected fitting model for unbiased STED-FCS analyses. *Methods*. doi: 10.1016/j.ymeth.2018.02.010 (2018).
45. Veerapathiran, S., Wohland, T. The imaging FCS diffusion law in the presence of multiple diffusive modes. *Methods*. doi: 10.1016/j.ymeth.2017.11.016 (2018).
46. Gupta, A., Phang, I.Y., Wohland, T. To hop or not to hop: exceptions in the FCS diffusion law. *Biophysical Journal*. doi: 10.1016/j.bpj.2020.04.004 (2020).

Figure 1

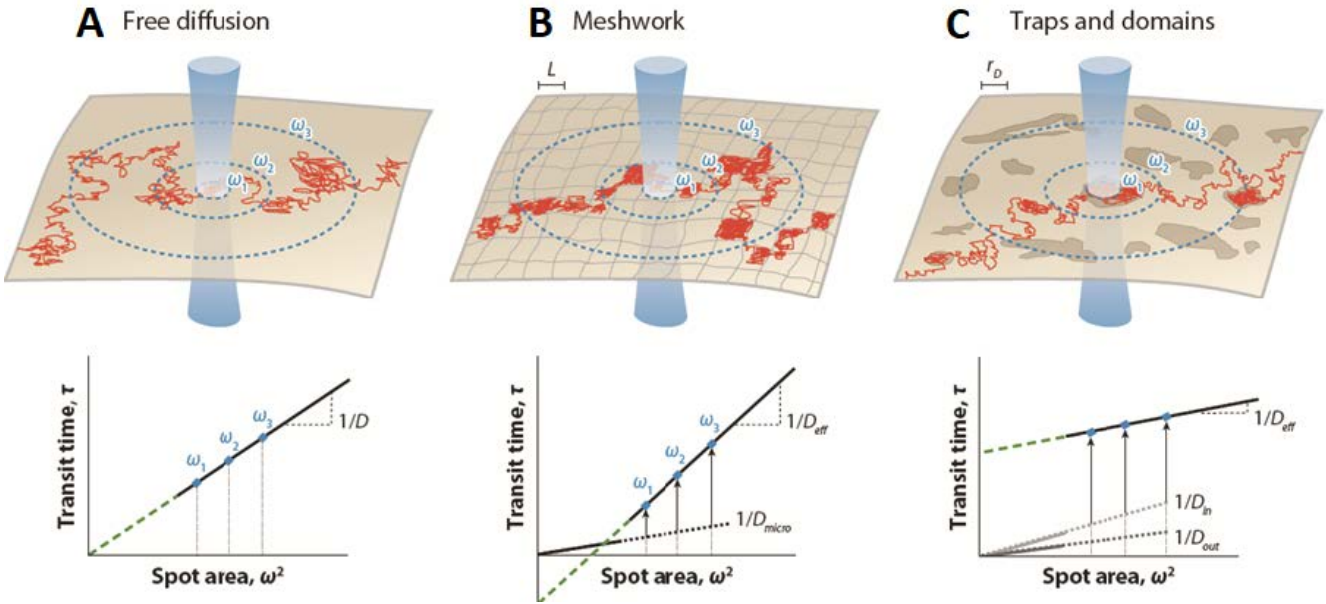

Figure 2

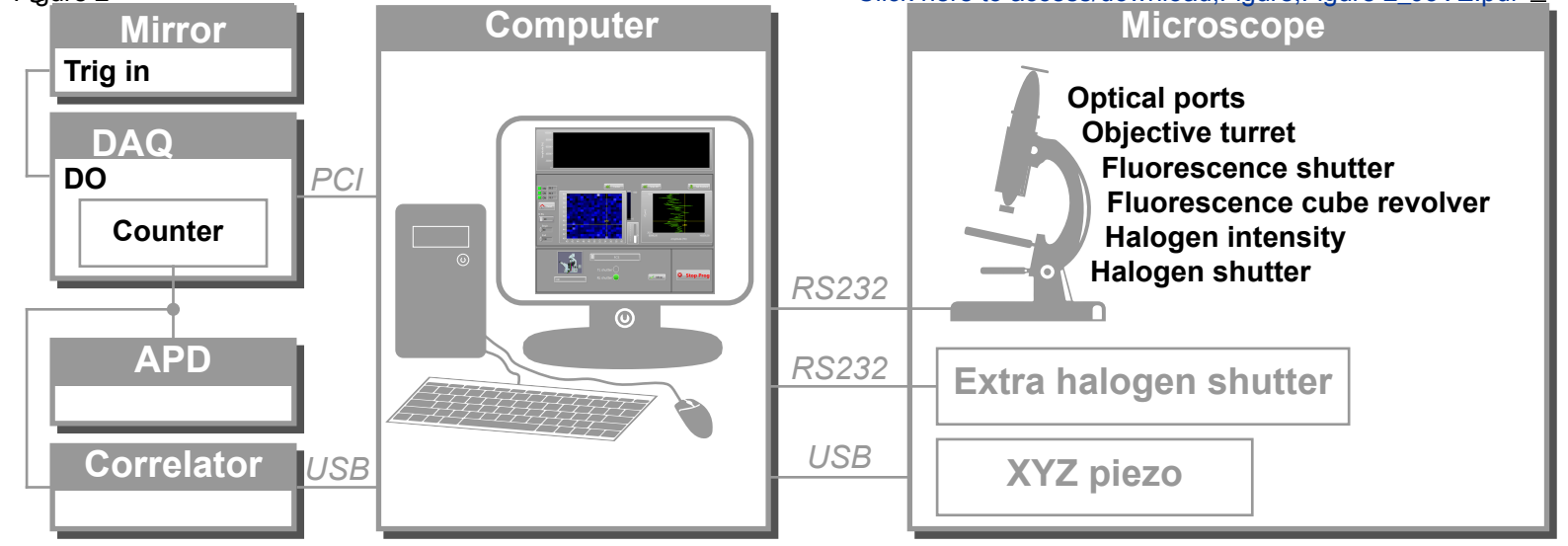

Figure 3

Click here to access/download;Figure;Figu

Optical table: 1000 x 1500

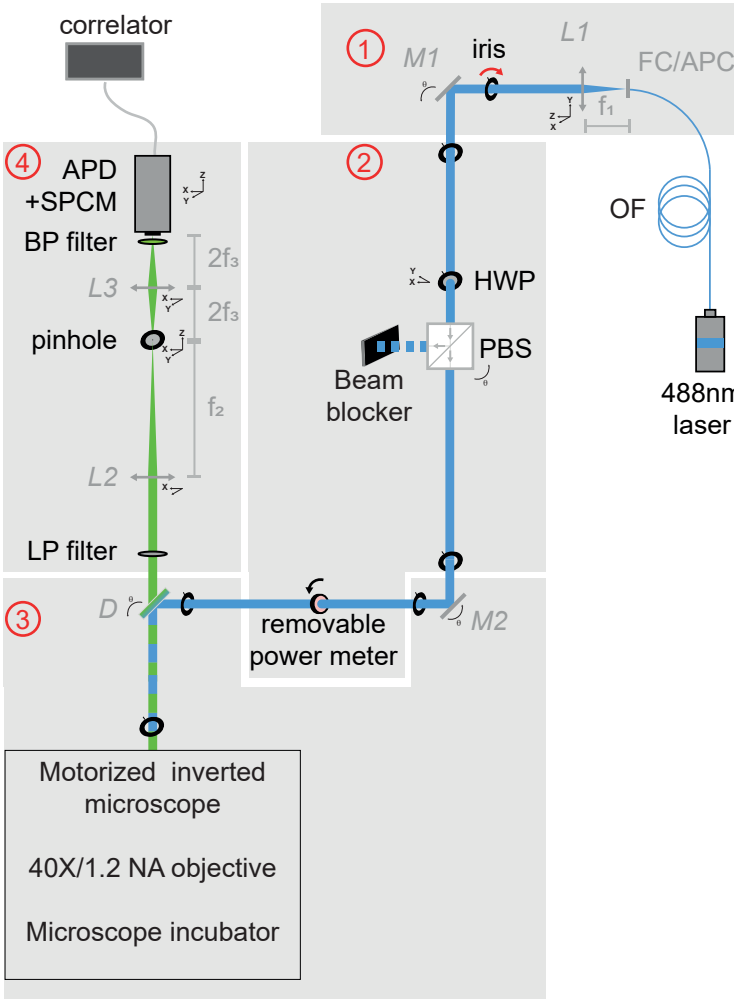

Figure 4

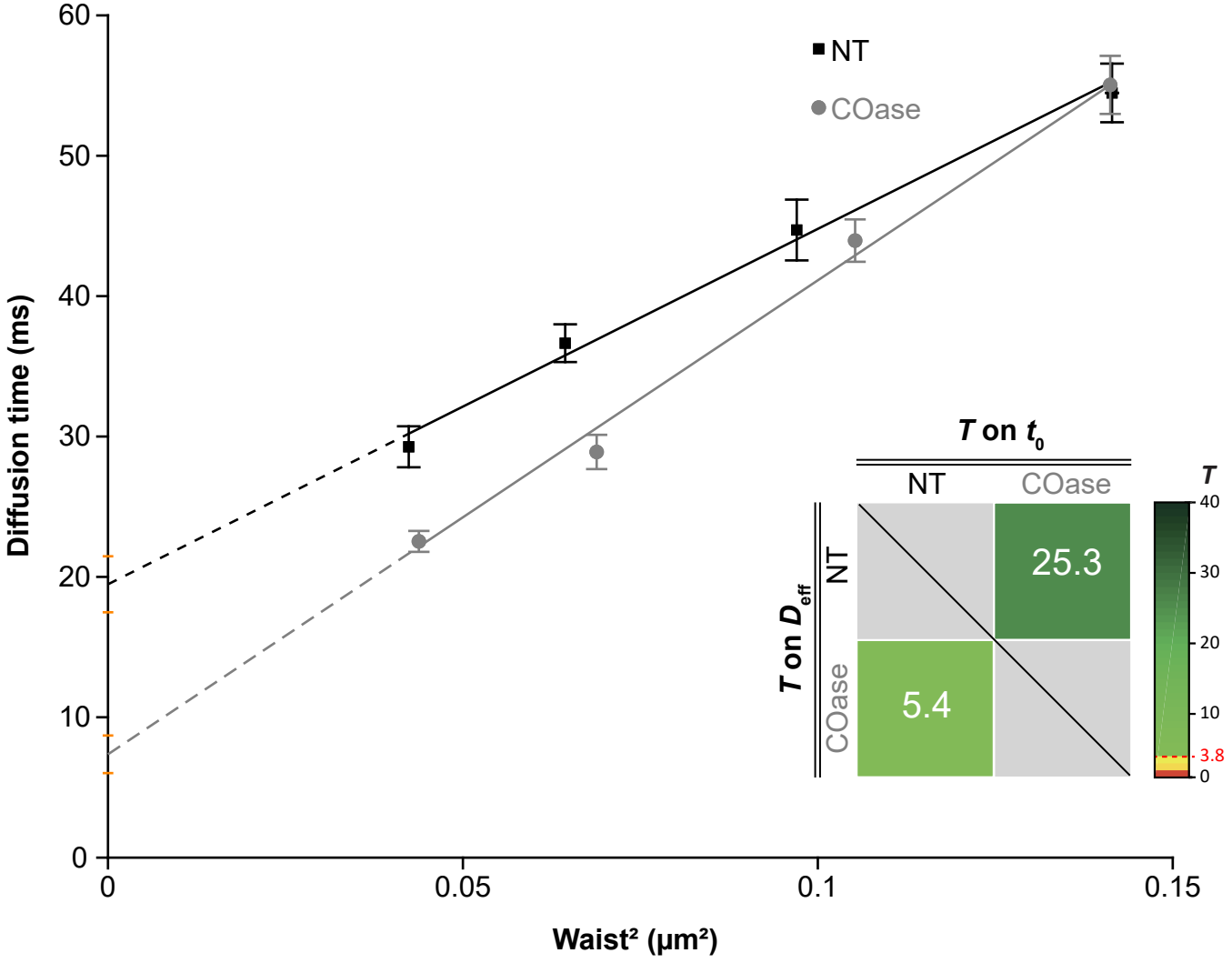

Figure 5

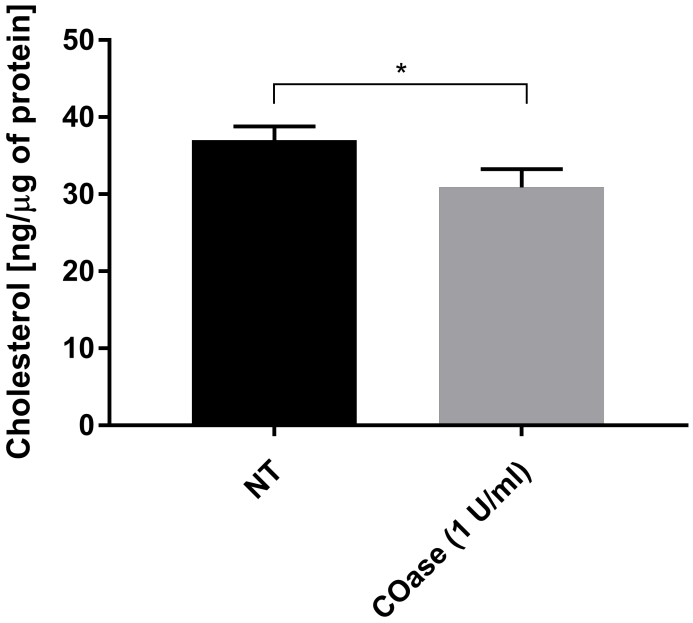

Table of Materials

Click here to access/download;Table of Materials;201012_JoVE_Table_of_Materials_final.xlsx

Comments/Description	Name of Material/Equipment	Company	Catalog Number
Aligment tool	Spanner Wrench for SM1-Threaded Retaining Rings	Thorlabs	SPW602
Avalanche Photodiode and Single Photon Counting Module (SPCM)	Single-Photon Counting Module, Avalanche Photodiode	Excelitas	SPCM-AQRH-15
	BNC 50 Ω plug to 50 Ω plug lead 2 m	RS Components	742-4315
	Coaxial cable 415 Cinch Connectors, RG-316, 50 Ω With connector, 1.22 m, RoHS2	RS Components	885-8172
	Tee 50Ω RF Adapter BNC Plug to BNC Socket 0 → 1GHz	RS Components	546-4948
	Brennenstuhl 2.5 m, 8 Socket Type E – French Extension Lead, 230 V	RS Components	768-5500
	Mascot, 6W Plug In Power Supply 5V dc, 1.2A, 1 Output Switched Mode Power Supply, Type C	RS Components	452-8394
	Crystek CCSMACL-MC-24 Reference Oscillator Power Cable RF Adapter	RS Components	792-4079
Fluorescence filtering	535/70 ET Bandpass, AOI 0° Chroma Diameter 25 mm	AHF filter	F47-539
	Laser Beamsplitter zt488 RDC, AOI 45° Chroma 25.5 x 36 x 1 mm	AHF filter	F43-088
	496/LP BrightLine HC Longpass Filter, AOI 0° Chroma Diameter 25	AHF filter	F37-496
Hardware correlator	80 MHz Digital Correlator	Correlator.com	Flex02-12D
Laser	LASER LASOS LDM-XT fiber coupled, 488 nm, 65 mW	Lasos	BLD-XT 488100
Laser safety	High-Performance Black Masking Tape, 1" x 180' (25 mm x 55 m) Roll	Thorlabs	T743-2.0
	Lens Tissues, 25 Sheets per Booklet, 5 Booklets	Thorlabs	MC-5
	Laser Safety Glasses, Light Orange Lenses, 48% Visible Light Transmission	Thorlabs	LG3B

Microscope	Zeiss Axiovert 200M Motorized Inverted Fluorescence Microscope Fine and coarse focusing, reflector turret rotation, objective nosepiece rotation, switching camera ports, and internal light shutters	Carl Zeiss	
	C-Apochromat 40x/1,2 W Korr.selected for FCS (D=0.14-0.19 mm) (WD=0.28 mm at D=0.17 mm), UV-VIS-IR	Carl Zeiss	421767-9971-711
	Adapter W0.8 / M27x0.75 H "5"	Carl Zeiss	000000-1698-345
	Middle ring W0.8 - W0.8 H "5"	Carl Zeiss	000000-1698-347
	D25.4mm Mirror, Protected Silver	Thorlabs	PF10-03-P01
	D25.4mm, F=60.0.mm, Visible Achromat	Thorlabs	AC254-060-A
	D25.4mm, F=35.0.mm, Visible Achromat	Thorlabs	AC254-035-A
	25 µm mounted pinhole	Thorlabs	P25S I
	25.4mm Mounted Zero, Order 1/2 Waveplate 488 nm	Thorlabs	WPH10M-488 (HWP)
	20mm Polarizing Beamsplitter Cube 420-680 nm	Thorlabs	PBS201
	Rotation Stage 56 mm x 26 mm Threaded ID	Thorlabs	RSP1/M
	52 mm x 52 mm Kinematic Platform Mount	Thorlabs	KM100B/M
	Adjustable Prism Clamp	Thorlabs	PM3/M
	Beam block - active area 19 mm x 38 mm	Thorlabs	LB1/M
	Iris Diaphragm 1 mm to 25 mm Aperture	Thorlabs	ID25/M
	Left-Handed Kinematic Cylindrical Lens Mount	Thorlabs	KM100CL
	1" Optic Holder, M4 Tap	Thorlabs	MFF101/M
	1" Stackable Lens Tube	Thorlabs	SM1L03
	Stackable Lens Mount for 1" optic-usable depth ½	Thorlabs	SM1L05
	Stackable Lens Mount For 1"Optic-usable Depth 2"	Thorlabs	SM1L20
	Small Optical Rails 600mm, metric	Thorlabs	RLA600/M
	Small Optical Rails 75mm, metric	Thorlabs	RLA075/M
	Small Optical Rails 150mm, metric	Thorlabs	RLA150/M
	Rail Carrier, Counterbored Hole 1"x 1"	Thorlabs	RC1
	Rail Carrier, Perpendicular Dovetail	Thorlabs	RC3

Optical path	High Precision Translating Lens Mount for 1 inch	Thorlabs	LM1XY/M
	½ " (12mm) Dovetail Translation Stage	Thorlabs	DT12/M
	Rail Clamps	Thorlabs	CL6
	Metric XYZ Translation Stage (Includes PT102)	Thorlabs	PT3/M
	Black Rubberized Fabric	Thorlabs	BK5
	Ball Driver kit/ 6 tools	Thorlabs	BD-KIT/M
	Adapter with External M6 x 1.0 Threads and External M4 x 0.7 Threads	Thorlabs	AP6M4M
	Mounting Base, 25 mm x 58 mm x 10 mm, 5 Pack	Thorlabs	BA1S/M-P5
	Lens Mount for 25.4mm optic	Thorlabs	LMR1/M
	SM1 FC/APC Adapter	Thorlabs	SM1FCA
	Kinematic Mirror Mount For 1 inch Optics	Thorlabs	KM100
	Silicon Power Head, 400-1100nm, 50mW	Thorlabs	S120C
	12.7 mm Post Holders, Spring-Loaded Hex-Locking Thumbscrew, L=50 mm, 5 Pack	Thorlabs	PH50/M-P5
	Post Holder with Spring-Loaded Hex-Locking Thumbscrew, L=20 mm	Thorlabs	PH20/M
	12.7 mm x 50 mm Stainless Steel Optical Post, M4 Stud, M6-Tapped Hole, 5 Pack	Thorlabs	TR50/M-P5
	12.7 mm x 75 mm Stainless Steel Optical Post, M4 Stud, M6-Tapped Hole, 5 Pack	Thorlabs	TR75/M-P5
	USB Power and Energy Meter Interface	Thorlabs	PM100USB
	12.7 mm x 30 mm Stainless Steel Optical Post, M4 Stud, M6-Tapped Hole	Thorlabs	TR30/M
	12.7 mm x 20 mm Stainless Steel Optical Post, M4 Stud, M6-Tapped Hole	Thorlabs	TR20/M
	750 mm long Structural Rail (detection box)	Thorlabs	XE25L750/M
	350 mm long Structural Rail (detection box)	Thorlabs	XE25L350/M
	Quick Corner Cube for 25 mm Rails	Thorlabs	XE25W3
	Right-Angle Bracket for 25 mm Rails	Thorlabs	XE25A90

	Black posterboard 20" x 30" (508 mm x 762 mm), 1/16" (1.6 mm) Thick, 5 Sheets	Thorlabs	TB5
	Hinge for 25 mm Rail Enclosures	Thorlabs	XE25H
	Lid Stop for 25 mm Rail Enclosures	Thorlabs	XE25LS
	M4 Cap Screw Kit	Thorlabs	HW-KIT1/M
	M6 Cap Screw Kit and Hardware kit	Thorlabs	HW-KIT2/M
	Table Clamp, L-Shape, 5 Pack	Thorlabs	CL5-P5
	SM1 Ring-Actuated Iris Diaphragm (Ø0.8 - Ø12 mm)	Thorlabs	SM1D12D
	Ø1" SM1-Mounted Frosted Glass Alignment Disk w/Ø1 mm Hole	Thorlabs	DG10-1500-H1-MD
	Honeycomb Optical Table Top, Standa	Standa	1HB10-15-12
	Optical Table support, Standa	Standa	1TS05-12-06-AR
Sample nano-positionning	Precision XYZ Nanopositioning	Physik Instrumente	PI P527-3.CD
	Digital Multi-Channel Piezo Co, 3 Channels, -30 to 130 V	Physik Instrumente	PI E727-3.CD
	Sub- D Connector(s), Capacitive Sensors,		
	ss 200M Inverted Microscope Incubator System MATT I	Digital Pixel	
Temperature chamber	Dual Channel Microprocessor Temperature Controller	Digital Pixel	DP_MTC_2000_DUO
	Two Vibration Free Heater Modules	Digital Pixel	DP_150_VF
	PT100 Temperature Sensor	Digital Pixel	DP_P100_TS
	Biological Reagents and Materials		
	Cos7 cells	ATCC®	CRL-1651™
	8- well Lab-Tek chambers	Thermo Fisher Scientific	155411PK
	Dulbecco's Modified Eagle Medium (DMEM)	Thermo Fisher Scientific	11965092
	Fetal bovine serum	Thermo Fisher Scientific	16000044
Cell culture and transfection	L-glutamine	Thermo Fisher Scientific	25030081
	PBS buffer	Thermo Fisher Scientific	14190144
	PenStrep	Thermo Fisher Scientific	15140122
	PolyJet Transfection Reagent	SignaGen Laboratories	SL100688

Cholesterol content measurement	Amplex Red Cholesterol Assay Kit	Thermo Fisher Scientific	A12216
	Protease Inhibitor Cocktail	Thermo Fisher Scientific	87786
	Phosphatase Inhibitor Cocktail	Thermo Fisher Scientific	78420
	ROTI Nanoquant Working Solution	Roth	K880
	GloMax Discover Microplate Reader	Promega	GM3000
svFCS measurements	HBSS buffer	Thermo Fisher Scientific	14025092
	Hepes buffer	Thermo Fisher Scientific	15630080
	Cholesterol oxidase	Sigma-Aldrich	C8868
	Rhodamine 6G	Sigma-Aldrich	83697-1G

Dear Editor,
Please find our revised manuscript with substantial improvements according to yours and reviewers' comments. As you have agreed, we removed the part of the protocol describing the construction of svFCS setup from the main manuscript and placed it as a supplementary material 1.
Below you will find our answers to your and reviewers' specific comments and suggestions.

Editorial comments:

Changes to be made by the Author(s):

1. Please take this opportunity to thoroughly proofread the manuscript to ensure that there are no spelling or grammar issues. The JoVE editor will not copy-edit your manuscript and any errors in the submitted revision may be present in the published version.
The manuscript was proofread, and we believe that we corrected all spelling and grammar mistakes.

2. Please format the manuscript as: paragraph Indentation: 0 for both left and right and special: none, Line spacings: single. Please include a single line space between each step, substep and note in the protocol section. Please use Calibri 12 points.
It has been done.

3. Please make the title concise.
We want to keep the title in the present form since it contains all the necessary information and illustrates the best the topic of our article. To make the title more concise, we could use the abbreviation of the method. However, we try to avoid writing svFCS since we think that the technique's full name is more informative for a broader audience.

4. Please provide at least 6 keywords or phrases.
It is the case.

5. Please ensure that the long Abstract is within 150-300-word limit and clearly states the goal of the protocol.
The Abstract has been adjusted.

6. JoVE cannot publish manuscripts containing commercial language. Please remove all commercial language from your manuscript and use generic terms instead. All commercial products should be sufficiently referenced in the Table of Materials and Reagents. For example: SI254, Thorlabs; SM1D12D, Thorlabs; 155411PK, Thermo Fisher; LabVIEW 2017 (National Instruments, Texas); (PCI-6602, National Instruments; Axiovert 200M (Carl Zeiss, Germany; Physik Instrumente (PI, Germany); Zeiss website; Uniblitz shutter (Vincent Associates, NY; Lab-Tek chambers (155411PK Thermo 432 Fisher); PolyJet Complexes; Gibco; Sigma-Aldrich; ROTI Nanoquant working solution (Roth); GloMax Discover Microplate Reader (Promega); etc.
It has been corrected.

7. Please ensure that all text in the protocol section is written in the imperative tense as if telling someone how to do the technique (e.g., "Do this," "Ensure that," etc.). The actions should be described in the imperative tense in complete sentences wherever possible. Avoid usage of

phrases such as “could be,” “should be,” and “would be” throughout the Protocol. Any text that cannot be written in the imperative tense may be added as a “Note.”
It has been corrected.

8. The Protocol should contain only action items that direct the reader to do something.
Yes, it does.

9. Please ensure you answer the “how” question, i.e., how is the step performed?
Yes, we did.

10. The Protocol should be made up almost entirely of discrete steps without large paragraphs of text between sections. Please simplify the Protocol so that individual steps contain only 2-3 actions per step. e.g., Step 2.
It has been corrected.

11. Please revise the protocol text to avoid the use of any personal pronouns in the protocol (e.g., "we", "you", "our" etc.).
It has been done.

12. Lines 288-294: We cannot have non numbered paragraphs in the protocol section. Please convert to numbered action step or a note under section 4.
It has been corrected.

13. In the JoVE Protocol format, “Notes” should be concise and used sparingly. They should only be used to provide extraneous details, optional steps, or recommendations that are not critical to a step. Any text that provides details about how to perform a particular step should either be included in the step itself or added as a sub-step.
Yes, we adapted to this format.

14. There is a 10-page limit for the Protocol (including single line space between each step), but there is a 2.75-page limit for filmable content. Please highlight 2.75 pages or less of the Protocol (including headings and spacing) that identifies the essential steps of the protocol for the video, i.e., the steps that should be visualized to tell the most cohesive story of the Protocol.
The limits are now respected.

15. Please obtain explicit copyright permission to reuse any figures from a previous publication. Explicit permission can be expressed in the form of a letter from the editor or a link to the editorial policy that allows re-prints. Please upload this information as a .doc or .docx file to your Editorial Manager account. The Figure must be cited appropriately in the Figure Legend, i.e. “This figure has been modified from [citation].”
According to the information on the Annual Reviews webpage (https://www.annualreviews.org/page/about/copyright-and-permissions), for the Annual Reviews Authors (dr D. Marguet in this case): There is no need to obtain permission from Annual Reviews for the use of your own work(s). Our copyright transfer agreement provides you with all the necessary permissions. Our copyright transfer agreement provides: “…The nonexclusive right to use, reproduce, distribute, perform, update, create derivatives, and make copies of the work (electronically or in print) in connection with the author’s teaching, conference presentations, lectures, and publications, provided proper attribution is given…”

16. Each Figure Legend should include a title and a short description of the data presented in the Figure and relevant symbols.
It has been corrected.

17. As we are a methods journal, please ensure that the Discussion explicitly cover the following in detail in 3-6 paragraphs with citations:

a) Critical steps within the protocol

b) Any modifications and troubleshooting of the technique

c) Any limitations of the technique

d) The significance with respect to existing methods

e) Any future applications of the technique

Additional improvements were made in the Discussion section to consider the aforementioned points.

18. Please do not abbreviate the journal titles in the references section.
It has been corrected.

19. Please sort the materials table in alphabetical order.
It has been done.

20. Table 1: Please upload in .xlsx format separately to your Editorial Manager account.
Yes.

Reviewer #1:

Manuscript Summary:

The article by Mailfert et al. describes the construction and usage of a confocal fluorescence correlation spectroscopy (FCS) setup with variable detection area to perform spot variation FCS. The setup is clearly described and should make it possible for the reader to construct such a system and operate it. I have some remarks, clarification of which might help reader.

Major Concerns:

One page 5 the authors write "The optimal is reached when the autocorrelation function shows the higher intensity count with the lower number of molecules present in the excitation volume (meaning the higher G0)."

Essentially the authors are saying the want to maximize the number of photon counts per particle and second. I would rewrite the phrase and say "The optimum is reached when one obtains the maximum counts per particle and second, i.e. a maximum correlation function

amplitude with high intensity." One also could point out that at the same time the diffusion time should be smallest.
We agree with the reviewer comment. The phrase has been changed accordingly (page 9 of the supplementary material 1).

Point 2.1.3: The authors mention that the reader should use a tube lens free microscope. But they also need to use lens L2 to create an intermediate image plane for the pinhole. Can one not use the microscope image plane after the tube lens to place the pinhole?
We thank the reviewer for this interesting remark. One can use the microscope image plane after the tube lens to place the pinhole. Two possibilities are then available: (1) a first requires separating the excitation and detection beams by using two microscope ports (e.g., rear and left port) or (2) if one wants to use a tube lens configuration, another possibility is to add an extra lens in the excitation path to keep the beam collimated and the back-pupil objective size. A paragraph has been added accordingly (page 7 of the supplementary material 1).

Some of the installation instructions are rather restrictive and could be loosened to give the protocol a wider range of applicability. E.g. under point 4 the authors ask for installations of 32 bit software on the basis that the microscope is controlled by 32 bit libraries. But this is not a state to exist for long and one wonders if it wouldn't be better to write this part more generally and that the user needs to adapt his software to the microscope with some details on what to watch out for?
We agree. The restriction about using a 32-bit version of Labview comes only from the fact that we use an old microscope driven by old 32-bit libraries. It was stated at page 1 of the supplementary material.

Under 10.6 the authors mention a software written for IGOR Pro. Is this software available to the readers? If yes, any restrictions on the version (32 bit or 63 but, 6,7,8 etc.)? If not, can it be any self-written software? In addition, one could point to already freely available software.
The fitting software was developed with IGOR Pro 6.37 32-bit and is available upon request through an MTA (Material Transfer Agreement). The 64-bit is not recommended by Wavemetrics as we are not working with extremely large data sets. The newer version of IGOR Pro (7 and 8) are also compatible with our software but request minor code modifications.
As the file provided by the correlator is in an easily readable format (text), the user can use any free software to load, discard, average fit, and analyse data.

Minor Concerns:

Line 50: replace "At first" with "First"

Line 74: replace "principal" with "important" or a synonym

Line 98: remove "a" before "a rapidly developing …"

Line 121: replace "… scratch custom …" with "… scratch a custom …"

Line 137: replace "optical path" with "optical axis"

Line 271: replace "eliminates" with "eliminate"

Line 385: remove the redundant "to the computer"

Line 487: delete "one of" in "at one of the maximal"

Line 566 onwards: Decimal points in numbers should be "." not ","
All have been corrected.

Reviewer #2:

Manuscript Summary:

The manuscript provides a useful protocol to assemble and employ a custom-built optical set up for spot variation FCS (svFCS) that is underpinned by a continuous wave laser, motorised inverted microscope, high NA water objective, an avalanche photodiode detector and a correlator, for live cell membrane studies. The microscopy set up is well described, however, the svFCS data acquisition and ACF analysis require more explanation. In particular, the details surrounding: (1) how the recorded fluctuations in fluorescence intensity are temporally segmented, (2) how the resulting autocorrelation functions (ACFs) are selected for averaging, and (3) how the ACF shape (diffusion time) changes as a function of spot radius; all need to be described and preferably visualised in a dedicated figure if the users of this protocol are going to be able to establish a diffusion law for molecules in the plasma membrane.
We agree with this comment, and we took into consideration the remarks when preparing the revised version of this manuscript. However, all the data acquisition steps were described in detail in our previous publication (Mailfert et al., 2017) together with appropriate figures, and we would not like to copy it in this manuscript to avoid redundancy.

In the Protocol under spot size calibration 10.5 and svFCS data acquisition 11.6 more detail should be provided on what is meant by '10 runs lasting for 20 seconds each' and '20 runs lasting for 5 seconds each'?
It has been addressed in point 8 of the revised Protocol.

For example what is the sampling frequency of these acquisitions (to emphasise what temporal resolution is required for a fast freely diffusing molecule like Rho6G versus a membrane protein like Thy-1-eGFP) and how many points are acquired in a trace (to emphasise the statistics required and the manner in which temporally you cut the data for the ACF analysis)?
The sampling frequency is determined by the hardware correlator, which provides a minimum sample time of 12.5ns (i.e., a sampling frequency of 80MHz), which is at least one thousand smaller than the resident time of freely diffusing Rho6G molecules (few tens of µs) and one million smaller than the diffusion of membrane protein within a 200 nm beam radius (discussed in the manuscript, section 3).

Also, what is the different between a run and a recording? If the run lasts for 5 seconds, how many points in time are acquired in this run? Is the 'recording' the acquisition time and then the 5 second 'runs' are the temporal segments used for the correlation analysis? If this is the case it would be good to provide this detail more accurately, and more importantly, provide commentary on why these parameters were selected (e.g. why 10 runs for 20 s for Rho6G and 20 runs for 5 s for Thy1-eGFP?).

We call a run a single measurement, providing a single ACF and recording a set of multiple runs. According to the multiple-tau correlation algorithm, the ACF provided by the real-time hardware correlator is composed of more than one thousand delay times logarithmically spaced between 12.5 ns to few seconds. It has been addressed in points 7 and 8 of the revised Protocol.

2. The information provided in 11.8 (four waste sizes varying between 200-400 nm) should be provided earlier in the protocol under spot size calibration 10.8 / svFCS data acquisition 11.7 and then further elaborated upon in terms of: (1) why were these parameters selected and (2) is there any point in going lower or higher than these waste values? In section 10.8 and 11.7 you are left wondering what sizes you should actually modulate the beam waste between and at what step size - for example what are the four wastes sizes between 200-400 nm that were employed and was this only because of optical limitations?
The waist size ranges from 200 to 400 nm only because of optical limitations (diffraction). By using different microscope objectives with different numerical apertures, we can modulate this range slightly.

3. In the Protocol under svFCS data analysis 12.1 it is stated that the users should 'select the individual autocorrelation functions characterised by the appropriate curve shape'. What is considered an 'appropriate' curve shape? Presumably, this point is meant to highlight that autocorrelation functions suffering from photobleaching or z drift will give rise to a slow a decay that extends out to 10 s and autocorrelation functions that don't detect the molecules will give rise to a correlation function that sharply decreases and potentially only contains correlation due to instrumentation effects. In either case what is 'appropriate' should be described more technically for users unfamiliar with ACF analysis and potentially there should be a figure dedicated to this since no ACF is shown in the protocol.
As stated previously, this critical step has been addressed in our previous publication (Mailfert et al., 2017). In the manuscript, we wrote the significant information according to the reviewer's comment (7.5, 7.11, 7.14, 8.9).

4. Given the points raised above (#2 and #3) it would be useful to generate a figure that describes the svFCS data acquisition and analysis. In particular present an example fluorescence fluctuation that was recorded, how this data is temporally segmented for ACF analysis, example ACF curves (appropriate and not appropriate), the average ACF curve fit to a 2D later diffusion model and extraction of the various parameters for establishing the diffusion law. In this figure it would also be particularly powerful to provide the average ACF curve derived as a function of spot waste so that users can see visually the impact this change in observation volume has on diffusion time.
As mentioned before, detailed figures describing these analyses were published within our previous publication (Mailfert et al., 2017). We would not like to copy it in this manuscript because of space limitations and to avoid redundancy.

5. In the protocol under svFCS data analysis there is no mention of how the ACF function amplitudes (G(0)) can be useful for determining the number or particles present in a selected single point measurement and how this information could be used in the context of svFCS to generate a concentration gradient. Potentially this avenue should be explored / presented or at least mentioned in the protocol text.

We added a comment in the manuscript's introduction to account for the comment about concentration measurement and in section 7.5.

Minor Concerns:

1. In the Protocol under svFCS data acquisition 11.5 it is unclear what is meant by the instructions on how to position the observation volume for the svFCS data measurement in the membrane of a selected cell. Why would it be preferable to run the scan in the nuclear area of the cell when the introduction of the protocol suggests the svFCS application here is for membrane-based studies? Potentially does this point mean to say the user should focus on the middle plane of the nucleus and then bring the focus down to where the nuclear envelope is no longer visible and Thy-1 eGFP extends to the perimeter of the cell.

It has been addressed in the revised Protocol, point 8.8.

2. In the Introduction it would be good to also mention spatiotemporal correlation spectroscopy (e.g. RICS, STICS, the pair correlation function, iMSD) alongside FRAP and FCS - as this family of methods also probe membrane diffusion with a spatial component introduced into the correlation function and like spot variant FCS (svFCS) that does this experimentally, reveal information concerning the underlying structure of the membrane. Then the high temporal resolution / statistics of svFCS compared to these spatiotemporal correlation-based approaches could be highlighted.

We agree that maybe it would be nice to introduce other methods. Still, we consider that this publication focuses on svFCS and its practical implementation. Taking into account the manuscript lenght, we did not introduced different methods in detail. In our opinion, there is no particular need to do so. However, we have mentioned some of the methods in the Discussion section.

3. In the introduction it should also be mentioned that the amplitude of the autocorrelation function can provide the number of particles present in the observation volume and how this parameter in the context of svFCS could provide information on the concentration gradient at any position interrogated.

It has been mentioned in the revised manuscript.

4. In the introduction at the top of page 2 the fluorescence signal is not 'induced' by diffusing fluorescent molecules but rather generated.

It has been corrected, thank you.

JOURNAL OF VISUALIZED EXPERIMENTS
1 Alewife Center #200
Cambridge, MA 02140
tel. 617.945.9051
www.jove.com

Supplementary Material – How to Build an svFCS Setup from Scratch

1. Experimental room requirement and safety

1.1. Install the system in a dark experimental room equipped with air conditioning at a stabilized temperature of ~21 °C and avoid direct airflow, at least on the optical table.

1.2. Use a passive or, if possible, an active optical table to reduce the impact of external vibrations transmitted through the ground.

1.3. Choose a matt black incubation chamber for the microscope equipped, if possible, with vibration-free heaters.

1.4. Install a warning indicating "Laser in use" at the room entrance and a laser interlock system for laser safety.

1.5. Wear laser safety goggles.

1.6. Use black laser curtains if several optical benches are in the same room.

1.7. Remove your watches, rings, or reflective objects during laser alignment.

2. Hardware and software installation and LabVIEW programming protocol

NOTE: The entire software is written in LabVIEW 2020 using a state machine and event structure architecture. The multifunction acquisition board (DAQ) drives most of the controllers. The correlator, laser, and power meter are controlled by their own software. Thus, this will not be discussed here. For the general operation scheme, see **Figure 2**.

2.1. Controller installation and configuration

2.1.1. LabVIEW and National Instruments products

2.1.1.1. Download and install the 2020 32-bit LabVIEW version (or newer), including NI-Visa (serial port communication) and VI Package Manager (VIPM, manage/update installed package) (ni.com). Update and upgrade all the features, to begin with, an up-to-date version via NI Update Service.

NOTE: As 32-bit dll libraries control our microscope, it is mandatory to use a 32-bit LabVIEW version. However, it can be adapted to the user's microscope.

2.1.1.2. Download and install NI-DAQmx 20.1 or newer (for data acquisition) by running the installation software provided with the acquisition board. These can be done directly with VIPM.

2.1.1.3. Activate your license with your National Instruments credentials.

2.1.1.4. Shut down the computer.

2.1.1.5. Plug the PCI-6602 DAQ card inside a free slot in the computer and plug the DAQ acquisition board (BNC-2121) to the PCI-6602 card with the 32-pin cable (any DAQ card with at least two counters and one digital input/output lines can be used).

2.1.1.6. Start the computer.

2.1.2. Piezoelectric XYZ nanopositioning stage

NOTE: This procedure will differ if you use a different controller from another company.

2.1.2.1. Insert the CD and launch "**PI_E-727.CD_Setup.exe**" and follow the procedure by using the default parameters.

NOTE: As we are using LabVIEW 32-bit, install the 32-bit version of the PI software and drivers.

2.1.2.2. When completed, launch "**PI Update Finder**" and click "**Find updates**" to download and update applications, drivers, and libraries.

2.1.2.3. Install the piezo XYZ stage (E-527.3CD) on your microscope stage (some mechanical adaptations should be required), connect the stage to its controller (PI-E727).

2.1.2.4. Plug the controller to the computer by using the USB cable and start it. The controller is driven by the LabVIEW using dedicated GSC libraries.

2.1.3. Microscope

32-bit dlls controls the microscope via LabVIEW through the RS232 COM port with the microscope.

NOTE: If you are using a different microscope, this procedure will differ.

2.1.3.1. To obtain the download link for the different installation programs, register on the website: https://www.zeiss.com/microscopy/int/downloads/micro-toolbox-mtb-.html.

2.1.3.2. Click on the "**MTB2004**" tab and download the 32-bit version of the software called "**MTB2004 RDK**" and "**MTB2004 SDK**" (MTB stands for MicroToolBox).

2.1.3.3. Click on the "**MTB**" tab and download the 32-bit software called "**Redistribution Kit**" and "**MTB Software Development**".

2.1.3.4. Unzip all the ZIP files and install the software following the different steps and keeping the default parameters.

2.1.3.5. Shut down the computer, plug your microscope with an RS232 cable to your computer, and restart both systems.

2.1.3.6. Execute the "**konfig.exe**" located into the "**Micro Toolbox**" folder in your hard drive). This is used to set the configuration of your microscope. Set the COM port number to which the microscope is connected, set the components installed on your microscope (motorized turrets, filter sets, objectives, etc.). Name this configuration by clicking on the "**Configuration tab**". Click on "**Exit**" and save this configuration.

2.1.3.7. Execute "**MTBConfig.exe**" located into the "**MTB 2004 – x.x\MTB Configuration**" folder. Select the COM port number (this should be the same on the computer and in the Config software), rename the configuration (not mandatory), and click on "**Auto Configuration**". The configuration will match exactly the one you set previously on "**Config.exe**". Any motorized component will be detected, and you can set non-motorized components manually.

2.1.3.8. Execute "**MTBTest.exe**" located into the "**MTB 2004 – x.x\MTB Test**" folder. Click on "**Build user interface**". A specific control interface will be created according to the previous configuration. It allows you to control and test all the motorized components of your microscope. Verify that everything is set and respond properly.

2.1.4. Correlator

2.1.4.1. Download the driver and software corresponding to your correlator model and operating system as ZIP file on the http://www.correlator.com/software website. The Windows 7 driver/program works with the Windows 10 OS.

2.1.4.2. Extract the files and place the corresponding folder anywhere on your hard drive (the execution file does not require to be installed in the "**Program Files**" Windows folder.

2.1.4.3. Plug the correlator to the computer by using a USB cable. As no driver was installed yet, the correlator will not be recognized if you open the Windows "**Device Manager**" program.

2.1.4.4. The correlator driver is not recognized as a "**signed driver**" by Windows 10. To install it, you should follow the Windows procedure to turn off driver signature verification: (1) Press and hold the Shift key on your keyboard and click the "**Restart**" button, (2) choose "**Troubleshoot | Advanced options | Startup Settings**" and (3) click the "**Restart**" button. (4) When your computer restarts, you will see a list of options, (5) Press F7 on your keyboard to select "**Disable driver signature enforcement**".

2.1.4.5. Now, install the driver located in the "**Correlator/driver**" folder: double click on the driver and follow the procedure.

2.1.5. Uniblitz shutter

The Uniblitz shutter, controlled via RS232 protocol, does not need any driver installation.

2.1.6. Power meter

NOTE: These steps are not mandatory if you use another power meter.

2.1.6.1. Extract the "**ThorlabsPowerMeter_1.0.2.zip**" (or newer version) file located in the USB provided with the power meter and double click on the "**Setup.exe**" installation program.

2.1.6.2. Install the software and drivers with the default installation options.

2.1.6.3. Plug the sensor on the power meter and then plug the power meter to the computer with a USB cable.

2.1.6.4. Launch the "**Optical Power Meter Utility.exe**" program located in the "**Thorlabs\PowerMeters**" folder: it should automatically detect your power meter through USB port communication.

2.1.7. Laser

NOTE: If your laser is not a LASOS laser, this procedure should be adapted.

2.1.7.1. Insert the USB key provided with the laser and launch the "**Setup.exe**" installation software located in the "**Software LASOS Commander 1.2\Installer**" folder. Follow the installation procedure and keep the default options.

2.1.7.2. Plug the laser to the computer to the computer using a USB cable.

2.1.7.3. Turn the interlock key to the "**1**" position.

2.1.7.4. Launch the laser software called "**LC.exe**" located in the "**LasosCommander**" folder.

2.1.7.5. Your laser should be automatically recognized.

2.1.8. Download and install the 6.37 32-bit version of IGOR Pro for data analysis. If one does not manage large datasets, the 64-bit version is not recommended. The newer version (7 and 8) of IGOR Pro are also compatible according to minor function modifications.

2.1.9. Download and install the latest MATLAB version for the diffusion law plot and comparison.

3. LabVIEW control software

3.1. LabVIEW: initialization steps

3.1.1. Initialize an NI-DAQmx task on a first counter (counter #0) to generate an acquisition clock with a fixed frequency and duty cycle.

3.1.2. Create a second counter (counter #1) task to effectively provide on request single photon counts whose clock is the output terminal of the first counter (each event received on the counter #1 between two clock pulses from the counter #0 are summed).

3.1.3. Generate a third task to create an asynchronous TTL digital output for the flipper mirror switch between its two states.

3.2. LabVIEW: state machine and event structures.

3.2.1. A while loop contains the two imbricated structures.

3.2.2. Any action on the graphical user interface (GUI) will generate a new state leading to an event. This allows the blocking of multiple events generation. Numerous GUI events can occur, each leading to a change in the state machine:

3.2.2.1. The default state is "Wait" where we monitor photon counts, while no event is recorded on the GUI.

3.2.2.2. "Mirror" event: when pressed or released, a boolean button leads to the generation of a TTL pulse on one digital output (DO) on the DAQ (a rising edge changes the state of the mirror), allowing the switching between the two states of the removable power meter sensor holder (i.e., in front of the beam for power measurement and laser safety or not for FCS measurement).

3.2.2.3. "Microscope" event: a specific command is sent through the RS232 port to control all the mechanical parts of the microscope (**Figure 2**).

3.2.2.4. In combination, an "external Uniblitz shutter" is controlled to match the microscope configuration to ensure that the halogen lamp is off during FCS acquisition.

3.2.2.5. For the piezo, three events can occur:

3.2.2.6. "2D scan": first, a matrix of NxM XY positions is created (according to the XY range and # of pixels). Thus, the piezo moves the sample at each XY position and the counter #0 task records the photon for each position: a 2D fluorescence confocal image is then created.

NOTE: This protocol is slow, and it uses NxM USB commands to be sent. A much faster protocol using analog signals can be used, but it requires a much more expensive multifunction acquisition board.

3.2.2.7. "Set position": The laser beam position on the sample is defined using a cursor placed on the 2D confocal image. This set the XY measurement position for the next step.

3.2.2.8. "1D scan": on the previously defined XY position, a Z-scan is performed, generally 20 steps over 20 µm, displaying a photon trace related to the fluorescence of the sample.

3.2.2.9. The autocorrelation function (ACF) is computed by the hardware correlator, meaning that the APD signal is also recorded on the correlator when required. This is performed with the correlator software.

4. Optical alignment steps (goggles required)

CAUTION: Never look directly into the beam path without laser safety goggles. Optical alignment should be performed by authorized people only.

4.1. Excitation part

The excitation part is composed of the laser collimation (line ①, **Figure 3**), a power control (line ②, **Figure 3**) and microscope coupling (line ③, **Figure 3**).

NOTE: We keep the same height for an entire optical path to avoid adding extra optical parts (adding potential mid-term misalignment, optimize the photon budget and possible optical aberrations). Here the height is 12 cm, given by 8 cm for the microscope left port plus 4 cm for the adjustable feet mounted under the microscope. These homemade adjustable feet allow correcting potential imperfections of the microscope itself.

4.1.1. The output of the laser fiber (screwed on the table) is designed to prevent back reflection of the beam into the laser (8° angle). It is connected to a threaded FC/APC adapter located at the focal plane of an achromatic doublet lens (L1). Alignment tools are used to center the beam on the lens, and the collimation is adjusted by moving the lens, thanks to a Z-axis translation. We used here a shearing interferometer to find the position where the beam was not convergent or divergent. The lens's horizontal tilt can be checked by looking at the beam back reflection, which has to coincide with the incident beam. A first iris allows adjusting the beam diameter to perform the spot variation FCS.

4.1.2. The M1 mirror is used to follow a line thanks to two irises screwed directly on the optical table (line ②, **Figure 3**) and centered at the height of 12 cm (one iris is located close to M1 and the second is close to the M2 mirror). Then, a zero-order half-wave plate (HWP) mounted in a rotation mount is placed and centered within the optical pathway (thanks to alignment tools). A 20 mm polarizing beam splitter cube (PBS) is added next to the half-wave plate to separate the s- and p-polarization components, reflecting the s component onto a beam-blocker and transmitting the p component. Therefore, the power is adjusted according to the half-wave plate axes' position and can be measured thanks to a flip mount where the power meter sensor is screwed. The power meter acts as a beam blocker; i.e., when no measurement on the sample is performed, the sensor is placed into the beam path, for laser and sample safety.

4.1.3. Then, M2 reflects the beam onto the dichroic mirror (DM) following a line of the optical table using two irises as described previously (line ③, **Figure 3**). Line ④ (**Figure 3**) is straight to the left port of the microscope. A reflective target is screwed onto the objective turret to finalize the alignment. The microscope is positioned so that the beam is centered onto the target thanks to translation in Y and adjustment of the height with the tunable homebuilt feet. The tilt is checked with the observation of the back reflection on the iris located in line ② (**Figure 3**) and corrected by adjusting the feet. Be sure to fasten the microscope securely to the optical table when the position is found. Fine adjustment can be made with M2 (target) and with DM (back reflection), alternatively.

NOTE: To optimize the photon budget and minimize optical aberrations, the microscope is tube-lens free. It should allow removing in the light path the tube-lens when the svFCS measurement is performed since the laser is already collimated and enter via the left port of the microscope. The 1X tube-lens is used only for cell visualization.

NOTE: To use a tube lens configuration to focus the beam directly through the pinhole, two possibilities are available: (1) a first requires separating the excitation and detection beams by

using two microscope ports (e.g., rear and left port) or (2), another possibility is to add an extra lens in the excitation path to keep the beam collimated and the back-pupil objective size.

4.1.4. The iris placed before M1 plays a key role in the svFCS setup as it changes the beam size before the objective, meaning that its size directly varies the effective waist size behind the objective, i.e., the effective excitation volume. This trivial option to tune the waist size ensures the optimization of the photon budget and is easy to implement. The beam diameter should fit the objective back pupil to obtain the smallest waist size[34].

1.1.5 Lab-Tek chambers were used for the measurements on cells. They are moved in by an XYZ piezo nanopositioning system, and a homemade sample holder supports the Lab-Tek.

4.2. Detection part

The detection part consists of two key components: the detection pinhole and the detector (**Figure 3**).

NOTE: The detection pinhole diameter should match the diameter of the Airy disc diffraction pattern and depends on the magnification and the numerical aperture (NA) of the objective lens as well as the emission wavelength. No additional magnification factor is added since the microscope is tube-lens free. The correction ring of the objective should be optimized to match the thickness of the coverslip used.

4.2.1. The objective lens can then be positioned and placed directly (to avoid ambiguity on the coverslip Z position). A droplet of water is added on it. It is covered with a coverslip to check the beam after focusing (it should be round and concentric). 200 µl of a concentrated solution of Rhodamine 6G (2–20 µM) are placed on the coverslip to align the detection pathway. The laser power should be increased until fluorescence is observed by eyes. Optical components after the dichroic mirror are mounted on a rail (line ④, **Figure 3**) to enable alignment along the optical axis (Z translation). A long-pass filter (LP filter) located after DM removes the remaining part of the laser light.

NOTE: We recommend to ask the manufacturer to provide the FCS-approved objective. We have already observed significant differences between objectives in terms of transmission and beam shape.

4.2.2. A lens (L2) is positioned close to the long pass filter and centered according to the fluorescence pathway. The collected signal is spatially filtered by a 25 µm pinhole located in the lens's focal plane. This step is challenging, and a bigger pinhole can be used first to find a good position and then replaced by the smaller one. A power meter placed behind the pinhole is useful to optimize the pinhole position in the XYZ axes.

4.2.3. The last step concerns the positioning of the avalanche photodiode (APD) detector coupled with a single photon counting module (SPCM), which shall remain switched off. A lens (L3) creates the image of the pinhole on the APD detection area. Note that the detection area should be bigger than the pinhole size to avoid the sectioning effect, i.e., the APD sensor's size should not act as a pinhole. The distance between the lens and the pinhole is, therefore, twice the focal distance and the distance between the lens and the APD (here, it is equal to 70 mm). A weak fluorescent spot can be seen on the detector and centered on the APD thanks to the APD XYZ-translation mount. A bandpass filter (BP filter) is placed in front of the detector to collect only the fluorescence signal. Once the rough alignment has been achieved, the Rh6G solution's concentration can be diluted (200 nM), the laser power reduced and the detector switched on. First, adjust the position of the APD by maximizing the count and then adjust the position of the pinhole in XYZ. Repeat the APD alignment to ensure that the pinhole is still imaged on the detector. A maximum count observed does not mean that it is a good position for the pinhole along the Z-axis; e.g., a high signal can come from the residual laser light. The best way to find the position is to perform an experiment with a more diluted sample and to record the autocorrelation function on the correlator. The optimum is reached when one obtains the maximum counts per particle and second (i.e., a maximum correlation function amplitude with high intensity [meaning the higher G(0))).